IEEE Access
Multidisciplinary ⋮ Rapid Review ⋮ Open Access Journal

Received August 9, 2019, accepted August 22, 2019, date of publication August 27, 2019, date of current version September 11, 2019.

Digital Object Identifier 10.1109/ACCESS.2019.2937915

3D Localization for Internet of Underground Things in Oil and Gas Reservoirs

NASIR SAEED, (Senior Member, IEEE), MOHAMED-SLIM ALOUINI, (Fellow, IEEE), AND TAREQ Y. AL-NAFFOURI, (Senior Member, IEEE)

Computer, Electrical, and Mathematical Sciences and Engineering (CEMSE) Division, King Abdullah University of Science and Technology (KAUST), Thuwal 23955-6900, Saudi Arabia

Corresponding author: Nasir Saeed (mr.nasir.saeed@ieee.org)

This work was supported by the Office of Sponsored Research (OSR) at King Abdullah University of Science and Technology (KAUST).

ABSTRACT Magnetic Induction (MI) is an efficient wireless communication method to deploy operational internet of underground things (IoUT) for oil and gas reservoirs. The IoUT consists of underground things which are capable of sensing the underground environment and communicating with the surface. The MI-based IoUT enable many applications, such as monitoring of the oil rigs, optimized fracturing, and optimized extraction. Most of these applications are dependent on the location of the underground things and therefore require accurate localization techniques. The existing localization techniques for MI-based underground sensing networks are two-dimensional and do not characterize the achievable accuracy of the developed methods, which are both crucial and challenging tasks. Therefore, this paper proposes a novel three-dimensional (3D) localization technique based on Isometric scaling (Isomap) for future IoUT. Moreover, this paper also presents the closed-form expression of the Cramer Rao lower bound (CRLB) for the proposed technique, which takes into account the channel parameters of the underground magnetic-induction. The derived CRLB provides the suggestions for an MI-based underground localization system by associating the system parameters with the error trend. Numerical results demonstrate that localization accuracy is affected by different channel and networks parameters such as the number of underground things, ranging error variance, size of the coils, and the transmitting power. The root mean square error performance of the proposed technique shows that increase in the number of turns of the coils, transmitting power, and the number of anchors improves the performance. Results also show that the proposed technique is robust to the ranging error variance in the range of 10 to 30 %; however, a further increase in the ranging error variance does not allow to achieve acceptable accuracy. Also, the results show that the proposed technique achieves an average of 30 % better localization accuracy compare to the traditional methods.

INDEX TERMS Magnetic induction, isometric scaling, internet of underground things, three-dimensional, localization, Cramer Rao lower bound.

I. INTRODUCTION

According to the report of the international energy agency (IEA), the energy needs of the world is expected to escalate by 40 % in 2030 (see Fig. 1) [1]. This ever-increasing demand for energy constitutes 20 % and 50 % escalation from the oil and gas industries, respectively. However, the operating environment of the oil and gas industries is challenging to fulfill this inexorable demand for energy [2]. One of the primary challenges of underground oil and gas reservoirs is to obtain their real-time information. This challenge can be addressed by using the internet of underground things (IoUT) which can optimize the production of oil and gas, monitor the flow of oil and gas, and can monitor the reservoir [3]. The IoUT based intelligent oil and gas fields can improve the accuracy, integrity, and timeliness of the production process [4].

Although IoUT enable multiple applications for underground oil and gas reservoirs, the challenging underground environment prevents the use of conventional terrestrial wireless communication systems. Therefore, magnetic-induction (MI) has emerged as a promising wireless communication technology to develop practical underground sensing

The associate editor coordinating the review of this article and approving it for publication was Sanket Goel.

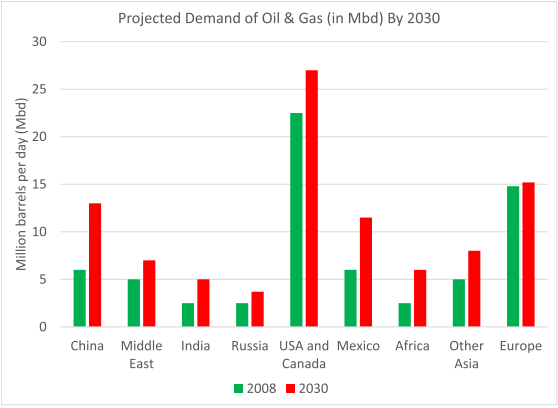

FIGURE 1. World projected energy demand by IEA.

systems [5]–[14]. MI uses time-varying magnetic fields to transmit the information in the underground environment. MI provides reliable and long-range communication in the underground environment as compared to its counterpart electromagnetic waves (EM) [15]. The performance of the EM in the underground is profoundly affected by properties of the subsurface environment such as soil structure, underground medium (soil, water, sand, etc.), and water contents [16]. However, all these impediments cause less attenuation to the MI-based communication systems. Besides, the EM-based systems require large size antennas for communication, which is impractical for the underground environment. Hence, MI-based systems are more practical because it relies on tiny size coil antennas.

Subsequently, efforts have been made in the recent past to develop MI-based underground sensing systems. However, most of the applications of the underground sensing systems such as monitoring of oil rig, optimized fracturing, and collecting of geo-tagged sensing data, require location information of the deployed sensors (underground things) [15], [17]. Therefore, the authors in [17] have proposed a localization scheme for underground sensing which utilizes the magnetic induction channel for distance estimation. The authors have used semi-definite programming (SDP) relaxation method for the distance estimation whereas the sensor nodes position is estimated by leveraging alternating direction augmented Lagrangian method (ADM) and conjugate gradient (CG) technique. The proposed solution in [17] is for two-dimensional underground sensing network while the three-dimensional (3D) nature of the underground environment requires 3D localization, which is more challenging. Moreover, the existing localization solutions do not consider the achievable accuracy for MI-based underground sensing systems, which is a crucial design parameter for any positioning system. Therefore, motivated by the above challenges, we present a novel MI-based 3D localization technique for the IoUT and provide the theoretical accuracy limit for the proposed technique. The major contributions of the paper are summarized as follows:

- A realistic 3D architecture of MI-based IoUT is presented for oil and gas reservoirs. Based on the 3D model, a novel localization technique is proposed which takes into account the noisy MI-channel based estimated distances and estimate the location of underground things. The positions estimated by Isometric scaling (Isomap) are refined by using a linear transformation technique.
- A closed-form expression for the Cramer Rao Lower bound (CRLB) is also derived for the proposed 3D MI-based IoUT localization technique. The derived lower bound is useful to compare the results of different MI-based underground localization systems.
- Numerical results are used to evaluate the performance of the proposed localization technique which is compared to the traditional methods and the derived CRLB, concerning different channel and network parameters such as range measurement errors, network size, and the number of anchors for MI-based IoUT.

The remainder of the paper is organized as follows. In section II and III, we present the related work and system model respectively. Section IV and V present the proposed 3D localization technique and formulation of the CRLB for MI-based IoUT, respectively. In section VI, we provide numerical results to validate the performance of the proposed technique. Finally, section VII concludes the paper.

II. RELATED WORK

The literature on localization techniques for terrestrial and underwater wireless networks is rich. In [18] and [19] classification of localization techniques for terrestrial and marine wireless networks is presented respectively where the localization schemes are categorized based on the type of computation (centralized/distributed), ranging technique (range-based/range-free), and space (2D/3D). However, the research work on the development of localization systems for the underground environment is limited due to numerous challenges such as non-availability of global positioning system (GPS) signals, high attenuation of radio frequency (RF) and electromagnetic (EM) waves, light-less environment, and narrow operational area. Even though localization techniques for GPS-denied environment such as underwater or indoor have been well developed, it is hard to apply those techniques to underground localization [3]. Both underwater and indoor localization techniques are based on either RF, acoustic, or optical signals [20]. However, the subsurface environment does not support the use of these signals, and therefore, the localization techniques developed for the underwater or indoor environment cannot be directly applied. Thus, a two-dimensional (2D) localization technique has been proposed in [17] for MI-based sensing networks. The authors in [17] have introduced the use of MI induction for channel-based distance estimation where the underground sensors were able to estimate the distances to their neighbors and the anchor nodes. Furthermore, a modified SDP relaxation-based technique is used, which jointly uses ADM and CG to determine the final position of the sensors.

However, in sparse underground sensing networks, the connectivity of the network is limited due to the short transmission distance of MI communication. Hence, localization of the underground things is challenging due to the limited connectivity, directionality of MI coils, interference from the Earth's magnetic field and underground metals [12], [21], [22]. Hence, in [15] the authors have investigated one of the challenges mentioned above, i.e., the impact of minerals and rocks on the MI-based underground localization. Attenuation properties have been estimated for different mediums in the underground, which significantly affects the performance of the localization techniques.

All of the above works consider two-dimensional localization for MI-based underground sensor networks. However, the subsurface environment is 3D and therefore requires 3D localization techniques. Furthermore, to the best of author's knowledge, the existing works do not characterize the achievable accuracy of the localization techniques. Therefore, motivated by the issues mentioned above, we propose a novel 3D dimensional localization technique, which is more realistic for the underground environment. The proposed 3D dimensional localization technique is based on Isomap, which is well-suited for 3D environments. Moreover, we also provide analysis for the proposed 3D localization technique for IoUT. Isomap-based proposed technique has better localization accuracy compare to its counterparts, weighted centroid (WC) [23], weighted-multidimensional scaling (WMDS) [24], and local linear embedding (LLE) [25] because the Isomap technique estimates the missing pairwise distance in three-dimensional space more accurately. The centroid localization techniques and its variants are not robust to the ranging errors and therefore yields low localization accuracy. Also, WC localization technique is center biased in nature, which results in a large localization error for the boundary nodes [23]. Moreover, they also require a large number of anchor nodes to improve the localization accuracy. On the other hand, WMDS and LLE provide an acceptable localization accuracy for two-dimensional networks since they are based on pairwise Euclidean distances. However, calculating the pairwise Euclidean distance in a three-dimensional network may not be a good approximation since Euclidean distance may fail to discover the nonlinear structure of the network. Also, the WMDS and LLE methods preserve the local structure, which reduces its complexity but may not guarantee global convergence and therefore requires the dense deployment of nodes in the network. Hence, we consider and Isomap based approach, which takes into account the 3D nature of the network by estimating the pairwise geodesic distances. Note that the proposed Isomap-based technique is centralized, which guarantees global convergence at the cost of high complexity.

Moreover, in the past, the estimation bounds for the time of arrival [26], the angle of arrival [27], time difference of arrival [28], and received signal strength [29] based localization techniques have been investigated. Subsequently, these findings have opened the door for developing accurate and robust localization algorithms. Therefore, we expect the same for our proposed lower bound for MI-based IoUT. The performance of the localization techniques is characterized by the CRLB, which is a non-linear estimation problem. Different CRLB analysis exists in the literature which not only depends on the ranging method but also depends on the other parameters such as multipath effect, number of anchors, and network type (single hop or multi-hop) [30]–[32]. Due to the simplicity and generic expressions of the CRLB, it is an attractive analyzing tool for localization systems. Therefore, in this paper, we derive the expression of the CRLB for MI-based IoUT localization, which takes into account the channel parameters of the underground magnetic-induction. The derived CRLB provides the suggestions for an MI-based underground localization system by associating the system parameters with the error trend. The proposed 3D localization technique and the derived expressions for the CRLB are general enough to be applicable for various multi-hop wireless communication networks. However, we primarily focused on multi-hop MI-based IoUT localization since we use the MI-based underground channel model for the range estimation. The received power that we utilize for the range estimation is based on the underground MI-communications.

III. SYSTEM MODEL

In this section, we first introduce the 3D architecture for MI-based IoUT. Then the wireless propagation model is presented for the distance estimation.

A. MI-BASED IOUT SETUP

We consider the conventional network setup for 3D MI-based IoUT which consists on N number of random underground things and M number of anchor nodes as shown in Fig. 2. The underground things are injected into the oil reservoir by using hydraulic fracturing [33], [34]. The underground things are uniformly distributed, and their positions are denoted by $\mathbf{S} = \{\mathbf{s}_i\}_{i=1}^{N}$ where $\mathbf{s}_i = \{x_i, y_i, z_i\}$ represents the 3D position of the i-th underground thing. As anchor nodes are necessary

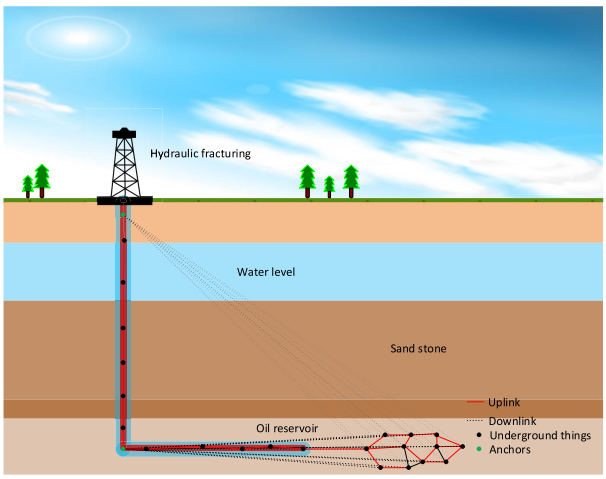

FIGURE 2. System model.

to find the position of the underground things, we assume that the anchor nodes are attached to the fracturing well with known positions $\{\mathbf{s}_j\}_{j=1}^{M}$ where $\mathbf{s}_j = \{x_j, y_j, z_j\}$ is the 3D position of the j-th anchor. The anchor nodes use large dipole antennas to communicate with the underground things by using the MI communication link. Hence, the downlink is a single hop channel (dotted black line in Fig. 2) while the underground things use multi-hop channel for the uplink transmission (solid red line in Fig. 2) due to their limited range. In practice, the transmission range of MI coils is enhanced by using the waveguide structure for coils [8]. Optimal deployment methods for underground waveguide structures were investigated in [8]. We also assume that the anchor nodes have higher transmission range as they can be attached to the external power sources [33]. The underground things can communicate to close by underground things and the anchors by using magnetic induction.

Based on the above network setup, the problem of localization is defined as, to estimate the unknown location of underground things for a given set of anchors and estimated MI-based distances. Note that the MI-based estimated distances between the underground things and the anchors are shared with a central node at the surface which computes the missing pairwise distances and determines the location of underground things. The centralized node at the surface creates a global map of the IoUT network with the location of each underground node.

B. MI-BASED UNDERGROUND DISTANCE ESTIMATION

The information exchange between the transmitting node and the receiving node in MI-based IoUT is accomplished by using a time-varying magnetic field which is produced by the modulated sinusoidal signal from the transmitter coil antenna. The time-varying magnetic field induces current at the receiver coil antenna which is demodulated to retrieve the information. Fig. 3 shows a realization of an MI-based transceiver. Consider that the current in the transmitting coil is $I = I_0\, e^{-j\omega t}$, where I_0 is the direct current, ω is the angular frequency, and t is the instantaneous time. This current can then induce current in the nearby coil by the phenomena of mutual induction. However, a single coil cannot guarantee to receive an MI signal if the receiving coil is not well coupled with the transmitting coil. Therefore, in the harsh underground environment, we assume the tri-directional coil receiver structure proposed in [9] for receiving strong MI

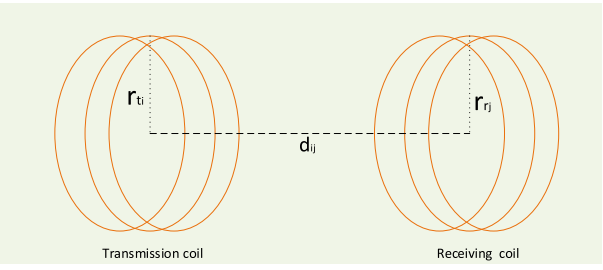

FIGURE 3. MI communication link.

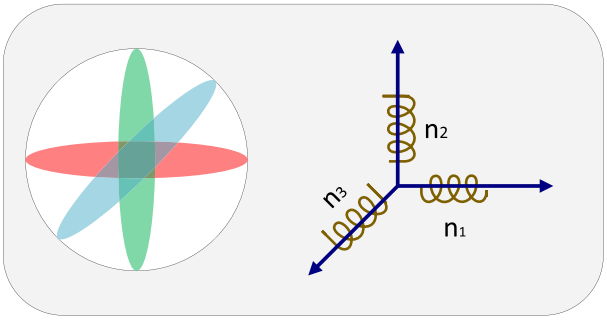

FIGURE 4. Tri-directional MI communication.

signal (see Fig 4). The advantage of using a tri-directional MI coil is that it provides omnidirectional coverage. The beams from each coil are pointed along each axis of the Cartesian coordinate system. Since the coils are orthogonal to each other and do not interfere with each other, the signals from all the three coils are combined at the receiver. Therefore, the impact of misalignment between the coils is minimized, such that the transmitted signal is received from at least a single coil [9].

Based on the magnetic induction, the relationship between the transmit and received power at high frequency f and large number of transmitter coil turns N_t is given in [35] as

$$P_{r_j} = \frac{\omega \mu P_{t_i} N_{r_j} N_{t_i} r_{t_i}^3 r_{r_j}^3 \sin^2 \alpha_{ij}}{16 R_0 d_{ij}^6}, \tag{1}$$

where ω is the angular frequency, μ is the permeability of soil, P_{t_i} is the transmit power, N_{r_j} is the number of turns in the receiver coil, r_{t_i} and r_{r_i} are the diameters of the transmitter and receiver coil respectively, α_{ij} is the angle between the axes of the transmitter and receiver coils, R_0 is the resistance of a unit length loop, and $d_{ij} = \| \mathbf{s}_i - \mathbf{s}_j \|$ is the distance between the transmitter and the receiver coil. The received power expression in (1) has been experimentally validated in [9]. Note that the path loss equation in (1) do not consider the effect of skin depth due to their little impact on the low carrier frequencies. However, in case of soil medium, the frequencies range is wide and therefore skin depth effect needs to be considered. Therefore, the distance between any two underground things in the presence of skin effect is written as

$$\hat{d}_{ij} = f(P_{r_j}) = \arg\left\{ d_{ij} | \Theta \right\} \tag{2}$$

where Θ is given in [17] as

$$\Theta = 10^{\frac{(P_{t_i} - P_{r_j})}{10}} - 1 = \frac{16 R_{0_t} R_{0_r} d_{ij}^3}{\omega^2 \mu^2 N_{t_i} N_{r_i} r_{t_i}^3 r_{r_j}^3 G^2(\sigma, \omega, d_{ij})}. \tag{3}$$

In (3) the term $G^2(\sigma, \omega, d_{ij})$ represents the loss due to skin depth where σ is the electrical conductivity of the soil.

IV. PROPOSED 3D LOCALIZATION TECHNIQUE

Based on the MI-based channel the distances between any two nodes i and j is estimated using (2). Since the transmission range of MI-links in the underground environment is

limited, each node can only estimate distance to the close by nodes. These single neighborhood distances are shared with the central station at surface. The central station employs a matrix completion strategy such as shortest path estimation to find the missing pairwise distance as follows:

$$\rho_{ij} = \begin{cases} \hat{d}_{ij} & \text{if } d_{ij} \leq d_m, \\ \hat{d}_{ih(1)} + \sum_{k=1}^{L-1} \hat{d}_{h(k),h(k+1)} + \hat{d}_{h(L)j} & \text{otherwise}, \end{cases} \tag{4}$$

where d_m is the maximum transmission distance of the coil, L represents the number of hops between node i and j whereas $h(1), \ldots, h(L)$ are the indices of the intermediate coils which are determined by the Dijkstra shortest path algorithm [36]. Here, for simplicity, we consider uniform power allocation for each underground coil for homogeneous connectivity. However, different power allocation strategies can be used, which can result in different magnetic vectors, generating a heterogeneous connected network [37]. The heterogeneous connected networks will require topology control mechanisms, such as the one in [38] and the references therein. The pairwise distances in (4) will significantly change in case of heterogeneous connectivity.

Collection of all the values of ρ_{ij} results in the following diagonal squared geodesic distance matrix (SGDM)

$$\Psi = \begin{bmatrix} 0 & \cdots & \rho^2_{i,(N+M)} \\ \vdots & \ddots & \vdots \\ \rho^2_{(N+M),1} & \cdots & 0 \end{bmatrix}. \tag{5}$$

Matrix Ψ is a square symmetric matrix where $\rho_{ij} = \rho_{ji}$ and $\rho_{ii} = 0$. Once matrix Ψ is formed, then dimensionality reduction techniques such as multidimensional scaling, principal component analysis, and Isomap can be used to visualize the high dimensional distances into low-dimensional coordinates [39]. In this paper, we use Isomap techniques because it is more suited for three-dimensional architectures [40]. Isomap tries to minimize the following cost function to reduce the high-dimensional estimated distances into three-dimensional lower space coordinates

$$\Phi(\mathbf{S}) = \sum_{ij} (\rho^2_{ij} - \parallel \mathbf{s}_i - \mathbf{s}_j \parallel^2), \tag{6}$$

where $\parallel \mathbf{s}_i - \mathbf{s}_j \parallel^2$ is the squared Euclidean distance between node i and j. Isomap tries to minimize the above cost function over all combinations of i and j. The analytical solution for the minimization of (6) does not exist. However, a gradient based minimization approach was proposed by Krusal in [41]. In Kruskal's approach, a centering operator $\mathbf{G} = \mathbf{I} - \frac{\mathbf{1}\mathbf{1}'}{\mathbf{1}'\mathbf{1}}$ is applied to the SGDM, i.e., $-\frac{1}{2}\mathbf{G}\Psi\mathbf{G}$, where $\mathbf{I}$ is the identity matrix and $\mathbf{1}$ is the vector of ones. The double centering operation subtracts the row and column means of a matrix from its elements and then adding the grand mean. This operation results in a double centered matrix, $\mathbf{H} = -\mathbf{G}\Psi\mathbf{G}^T/2$, where the elements of $\mathbf{H}$ are given as

$$h_{ij} = -0.5\left(\rho^2_{ij} - \frac{1}{T}\sum_{i=1}^{T}\rho^2_{ij} - \frac{1}{T}\sum_{j=1}^{T}\rho^2_{ij} - \frac{1}{T^2}\sum_{i=1}^{T}\sum_{j=1}^{T}\rho^2_{ij}\right), \tag{7}$$

where $T = N + M$. Taking the Eigenvalue decomposition of $\mathbf{H}$ yields

$$\tilde{\mathbf{S}} = \mathbf{V}\sqrt{\mathbf{U}}, \tag{8}$$

where $\mathbf{V}$ and $\mathbf{U}$ are the eigenvectors and eigenvalues of $\mathbf{H}$ respectively. The dimensions of $\mathbf{V}$ and $\mathbf{U}$ are $T \times 3$ and 3×3 respectively, for 3D estimation. $\tilde{\mathbf{S}}$ is a $T \times 3$ matrix where each row represents the 3D coordinate of a node with respect to other nodes in the network. Note that the 3D coordinates are relative to each other and do not have an actual coordinate system. To convert these local coordinates of the nodes to geographic coordinates, linear transformation techniques such Helmert transformation [42] or Procrustes analysis [43] is used. Based on the anchor positions and linear transformation, the location of the nodes are estimated as follows:

$$\hat{\mathbf{S}} = \varpi\, \varsigma(\tilde{\mathbf{S}}) + \tau \tag{9}$$

where ϖ, ς, and τ are the rotation, scaling, and translation factors respectively. These transformation elements mainly rely on the total number of anchors and their locations. Consider that the real location of anchor nodes is $\mathbf{S}_a = \{\mathbf{s}_1, \mathbf{s}_2, \ldots \mathbf{s}_M\}$ and their estimated locations are $\tilde{\mathbf{S}}_e = \{\tilde{\mathbf{s}}_1, \tilde{\mathbf{s}}_2, \ldots \tilde{\mathbf{s}}_M\}$, then cost function for the Procrustes analysis is defined as

$$f(\varpi, \tau, \varsigma) = \sum_{i=1}^{M} (\tilde{\mathbf{s}}_i - \varsigma\varpi^T\mathbf{s}_i - \tau)^T \times (\tilde{\mathbf{s}}_i - \varsigma\varpi^T\mathbf{s}_i - \tau) \tag{10}$$

The optimal values of ϖ, τ, and ς is obtained by minimization of (10). To minimize (10), we consider that $\mathbf{c}_a = \frac{1}{M}\sum_{i=1}^{M}\mathbf{s}_i$ and $\mathbf{c}_e = \frac{1}{M}\sum_{i=1}^{M}\hat{\mathbf{s}}_i$ as the centroid of the real and estimated location of anchor nodes, respectively. Putting the values of $\mathbf{c}_a$ and $\mathbf{c}_e$ in (10) yields

$$\begin{aligned} f(\varpi, \tau, \varsigma) = \sum_{i=1}^{M} \Big(& (\tilde{\mathbf{s}}_i - \mathbf{c}_e) - \varsigma\varpi^T(\mathbf{s}_i - \mathbf{c}_a) \\ & + \tilde{\mathbf{s}}_i - \varsigma\varpi^T\mathbf{s}_i - \tau \Big)^T \\ & \times \Big((\tilde{\mathbf{s}}_i - \mathbf{c}_e) - \varsigma\varpi^T(\mathbf{s}_i - \mathbf{c}_a) \\ & + \tilde{\mathbf{s}}_i - \varsigma\varpi^T\mathbf{s}_i - \tau \Big). \end{aligned} \tag{11}$$

Solving (11) yields optimal τ as follows

$$\tau = \mathbf{c}_e - \varsigma\varpi^T\mathbf{c}_a. \tag{12}$$

Considering that $\mathbf{c}_e = \mathbf{c}_a = 0$ and putting τ in (11) yields

$$f(\varpi, \tau, \varsigma) = \sum_{i=1}^{M} (\tilde{\mathbf{s}}_i - \varsigma \varpi^T \mathbf{s}_i)^T (\tilde{\mathbf{s}}_i - \varsigma \varpi^T \mathbf{s}_i). \quad (13)$$

It is worthy to note that the function in (13) is convex. Therefore, the optimal value of ς is obtained by differentiating (13) with respect to ς as follows

$$\varsigma = \frac{\mathrm{Tr}\left(\mathbf{S}_a \varpi \tilde{\mathbf{S}}_e^T\right)}{\mathrm{Tr}\left(\mathbf{S}_a \tilde{\mathbf{S}}_e^T\right)} \quad (14)$$

where $\mathrm{Tr}(\cdot)$ represents the trace operator. Finally, the optimal value of ϖ is obtained from the Eigenvalue decomposition of $\mathbf{S}_a \tilde{\mathbf{S}}_e^T$. Major steps of the proposed localization technique are described in algorithm 1.

Algorithm 1 Proposed Isomap Based Localization Algorithm

Input: Single hop noisy geodesic distances $\hat{d}_{ij}$ and set of anchors
Output: Location estimation of all the underground nodes, i.e., $\hat{\mathbf{S}}$
1: Compute the SGDM matrix Ψ by using (5)
2: Use (4) to estimate the missing geodesic pairwise distances
3: Use (8) to estimate the initial position of the underground sensors
4: Use Procrustes analysis to get the final estimated location by using (9)
5: **return**: Location estimations $\hat{\mathbf{S}}$

V. THEORETICAL ANALYSIS

In this section, we analyze the performance of the proposed localization method by deriving the lower bound for the error variance, i.e., the CRLB. The achievable accuracy of any localization technique can be characterized by the CRLB. Therefore, in this section we derive the closed form expression for the MI-based IoUT localization. As, the received power for MI-links is affected by the background noise b_{ij} which is modelled as zero mean Gaussian random variable with variance σ_{ij}^2 [9]. The probability density function (PDF) of the noisy received power $\tilde{P}_{r_j}$ is written as

$$f(\tilde{P}_{r_j}|\mathbf{s}_i, \mathbf{s}_j) = \frac{1}{\sigma_{ij}\sqrt{2\pi}} \exp\left(-\frac{(\tilde{P}_{r_j} - P_{r_j})^2}{2\sigma_{ij}^2}\right). \quad (15)$$

Based on the above PDF, the derivation of the CRLB consists of the following steps.

1) LOG-LIKELIHOOD RATIO CALCULATION

The concept of log-likelihood function is used in various signal processing applications to compute the Fisher information matrix (FIM) for estimation and detection [44]. The log-likelihood ratio is calculated from the PDF in (15) as follows:

$$\ell[dB] = -\log(\sigma_{ij}\sqrt{2\pi}) + \log\left(\exp^{-\frac{(\tilde{P}_{r_j} - P_{r_j})^2}{2\sigma_{ij}^2}}\right). \quad (16)$$

However, computing the FIM from the log-likelihood function is a challenging task, particularly when it is intractable [44]. Therefore, in most of the cases, the log-likelihood function is calculated by assuming that the ranging information is an independent and identically distributed (i.i.d) random variable [45]. Hence, The joint log-likelihood ratio for all the underground things is given as

$$\mathbf{L} = \sum_{i=1}^{N}\sum_{j=1}^{M} \log\left(f(\tilde{P}_{r_j}|\mathbf{s}_i, \mathbf{s}_j)\right). \quad (17)$$

2) COMPUTATION OF THE FISHER INFORMATION MATRIX

FIM tells us about how much information (localization accuracy) can be achieved from the noisy received power [46]. The FIM constitutes of sub-matrices for the three-dimensional location estimation given as

$$\mathbf{I} = \begin{bmatrix} \mathbf{I}_{x,x} & \mathbf{I}_{x,y} & \mathbf{I}_{x,z} \\ \mathbf{I}_{x,y}^T & \mathbf{I}_{y,y} & \mathbf{I}_{y,z} \\ \mathbf{I}_{x,z}^T & \mathbf{I}_{y,z}^T & \mathbf{I}_{z,z} \end{bmatrix}. \quad (18)$$

The elements of the sub-matrices in FIM are derived from the second order derivatives of the log-likelihood function defined in (17). The elements of the sub-matrices are calculated as

$$\mathbf{I}_{x,x_{i=l}} = E\left(\frac{\partial^2 \ell_{ij}}{\partial x_i^2}\right), \quad (19)$$

$$\mathbf{I}_{x,y_{i=l}} = E\left(\frac{\partial^2 \ell_{ij}}{\partial x_i y_i}\right), \quad (20)$$

$$\mathbf{I}_{x,z_{i=l}} = E\left(\frac{\partial^2 \ell_{ij}}{\partial x_i z_i}\right), \quad (21)$$

$$\mathbf{I}_{y,y_{i=l}} = E\left(\frac{\partial^2 \ell_{ij}}{\partial y_i^2}\right), \quad (22)$$

$$\mathbf{I}_{y,z_{i=l}} = E\left(\frac{\partial^2 \ell_{ij}}{\partial y_i z_i}\right), \quad (23)$$

and

$$\mathbf{I}_{z,z_{i=l}} = E\left(\frac{\partial^2 \ell_{ij}}{\partial z_i^2}\right), \quad (24)$$

respectively. Similarly, the non-diagonal elements are given as

$$\mathbf{I}_{x,x_{i\neq l}} = E\left(\frac{\partial^2 \ell_{ij}}{\partial x_i x_l}\right), \quad (25)$$

$$\mathbf{I}_{x,y_{i\neq l}} = E\left(\frac{\partial^2 \ell_{ij}}{\partial x_i y_l}\right), \quad (26)$$

$$\mathbf{I}_{x,z_{i\neq l}} = E\left(\frac{\partial^2 \ell_{ij}}{\partial x_i z_l}\right), \quad (27)$$

$$\mathbf{I}_{y,y_{i\neq l}} = E\left(\frac{\partial^2 \ell_{ij}}{\partial y_i y_l}\right), \tag{28}$$

$$\mathbf{I}_{y,z_{i\neq l}} = E\left(\frac{\partial^2 \ell_{ij}}{\partial y_i z_l}\right), \tag{29}$$

and

$$\mathbf{I}_{z,z_{i\neq l}} = E\left(\frac{\partial^2 \ell_{ij}}{\partial z_i z_l}\right), \tag{30}$$

where $E(\cdot)$ is the expectation operator. To derive the diagonal elements of each sub-matrix, we put the value of P_{r_j} in the above sub-matrices and solve it. Expression for the diagonal elements are obtained in Appendix A as follows

$$\mathbf{I}_{x,x_{i=l}} = \frac{3k}{\sigma_{ij}^2}\left(\frac{2k}{\| \mathbf{s}_i - \mathbf{s}_j \|^7} - \frac{28k(x_i - x_j)^2}{\| \mathbf{s}_i - \mathbf{s}_j \|^8} + \frac{k}{\| \mathbf{s}_i - \mathbf{s}_j \|^7} - \frac{8(x_i - x_j)^2)}{\| \mathbf{s}_i - \mathbf{s}_j \|^5}\right) \tag{31}$$

$$\mathbf{I}_{x,y_{i=l}} = \frac{60\, k^2 (x_i - x_j)(y_i - y_j)}{\sigma_{ij}^2 \| \mathbf{s}_i - \mathbf{s}_j \|^8}, \tag{32}$$

$$\mathbf{I}_{x,z_{i=l}} = \frac{60\, k^2 (x_i - x_j)(z_i - z_j)}{\sigma_{ij}^2 \| \mathbf{s}_i - \mathbf{s}_j \|^8}, \tag{33}$$

$$\mathbf{I}_{y,y_{i=l}} = \frac{3k}{\sigma_{ij}^2}\left(\frac{2k}{\| \mathbf{s}_i - \mathbf{s}_j \|^7} - \frac{28k(y_i - y_j)^2}{\| \mathbf{s}_i - \mathbf{s}_j \|^8} + \frac{k}{\| \mathbf{s}_i - \mathbf{s}_j \|^7} - \frac{8(y_i - y_j)^2)}{\| \mathbf{s}_i - \mathbf{s}_j \|^5}\right) \tag{34}$$

$$\mathbf{I}_{y,z_{i=l}} = \frac{60\, k^2 (y_i - y_j)(z_i - z_j)}{\sigma_{ij}^2 \| \mathbf{s}_i - \mathbf{s}_j \|^8}, \tag{35}$$

and

$$\mathbf{I}_{z,z_{i=l}} = \frac{3k}{\sigma_{ij}^2}\left(\frac{2k}{\| \mathbf{s}_i - \mathbf{s}_j \|^7} - \frac{28k(z_i - z_j)^2}{\| \mathbf{s}_i - \mathbf{s}_j \|^8} + \frac{k}{\| \mathbf{s}_i - \mathbf{s}_j \|^7} - \frac{8(z_i - z_j)^2)}{\| \mathbf{s}_i - \mathbf{s}_j \|^5}\right) \tag{36}$$

where $k = \frac{\omega \mu P_{t_i} N_{r_j} r_{t_i}^3 r_{r_j}^3 \sin^2 \alpha_{ij}}{16\, R_0\, G^2(\sigma,\omega,d_{ij})}$. Similarly solving (25) to (30) for the non-diagonal elements yields

$$\mathbf{I}_{x,x_{i\neq l}} = -\frac{3k}{\sigma_{ij}^2}\left(\frac{2k}{\| \mathbf{s}_i - \mathbf{s}_j \|^7} - \frac{28k(x_i - x_j)^2}{\| \mathbf{s}_i - \mathbf{s}_j \|^8} + \frac{k}{\| \mathbf{s}_i - \mathbf{s}_j \|^7} - \frac{8(x_i - x_j)^2)}{\| \mathbf{s}_i - \mathbf{s}_j \|^5}\right) \tag{37}$$

$$\mathbf{I}_{x,y_{i\neq l}} = -\frac{60\, k^2 (x_i - x_j)(y_i - y_j)}{\sigma_{ij}^2 \| \mathbf{s}_i - \mathbf{s}_j \|^8}, \tag{38}$$

$$\mathbf{I}_{x,z_{i\neq l}} = -\frac{60\, k^2 (x_i - x_j)(z_i - z_j)}{\sigma_{ij}^2 \| \mathbf{s}_i - \mathbf{s}_j \|^8}, \tag{39}$$

$$\mathbf{I}_{y,y_{i\neq l}} = -\frac{3k}{\sigma_{ij}^2}\left(\frac{2k}{\| \mathbf{s}_i - \mathbf{s}_j \|^7} - \frac{28k(y_i - y_j)^2}{\| \mathbf{s}_i - \mathbf{s}_j \|^8} + \frac{k}{\| \mathbf{s}_i - \mathbf{s}_j \|^7} - \frac{8(y_i - y_j)^2)}{\| \mathbf{s}_i - \mathbf{s}_j \|^5}\right) \tag{40}$$

$$\mathbf{I}_{y,z_{i\neq l}} = -\frac{60\, k^2 (y_i - y_j)(z_i - z_j)}{\sigma_{ij}^2 \| \mathbf{s}_i - \mathbf{s}_j \|^8}, \tag{41}$$

and

$$\mathbf{I}_{z,z_{i\neq l}} = -\frac{3k}{\sigma_{ij}^2}\left(\frac{2k}{\| \mathbf{s}_i - \mathbf{s}_j \|^7} - \frac{28k(z_i - z_j)^2}{\| \mathbf{s}_i - \mathbf{s}_j \|^8} + \frac{k}{\| \mathbf{s}_i - \mathbf{s}_j \|^7} - \frac{8(z_i - z_j)^2)}{\| \mathbf{s}_i - \mathbf{s}_j \|^5}\right). \tag{42}$$

Substituting the values of (31) to (42) in (18) completes the FIM.

3) CRAMER RAO LOWER BOUND

Finally the CRLB is calculated from the inverse of the FIM which is given as

$$\text{CRLB} = \mathbf{I}_{x,x}^{-1} + \mathbf{I}_{y,y}^{-1} + \mathbf{I}_{z,z}^{-1}. \tag{43}$$

Thus, we have developed a generalized CRLB for MI-based IoUT which is the function of different channel and network parameters such as operating frequency, number of turns of the coils, radius of the coils, transmit power, noise variance, number of anchors, and number of underground things. The derived CRLB provide the suggestions for an MI-based underground localization system by associating the channel and network parameters with the error trend.

VI. NUMERICAL RESULTS

In this section, we provide numerical results to validate the performance of the proposed 3D localization technique and compare with the derived CRLB, in a 3D underground oil reservoir setup. The performance of the proposed technique for MI-based IoUT is tested under various network settings.

A. SIMULATION PARAMETERS

We consider a 15 × 15 m^3 cubic fracture with 60 nodes randomly and uniformly distributed as shown in Fig. 5. Table 1 presents the simulation parameters which are taken mainly from [17]. Also, we consider the practical value of average temperature for the underground oil and gas reservoirs, i.e., 145° [47]. The results are also compared to well-known network localization techniques such as weighted centroid [23], weighted-multidimensional scaling [24], and local linear embedding [25]. In the following, first, we examine the effect of noise variance on the performance of the CRLB. Then, we evaluate the performance regarding the number of turns of the coils, coils size, and transmit power. Root mean square positioning error (RMSPE) is considered as an evaluation metric for all the simulations which is given as

$$\text{RMSPE} = \sqrt{\frac{\sum_{i=1}^{N} (\hat{x}_i - x_i)^2 + (\hat{y}_i - y_i)^2 + (\hat{z}_i - z_i)^2}{N}}, \tag{44}$$

where $\{x_i, y_i, z_i\}$ and $\{\hat{x}_i, \hat{y}_i, \hat{z}_i\}$ are the actual and estimated position of node i respectively.

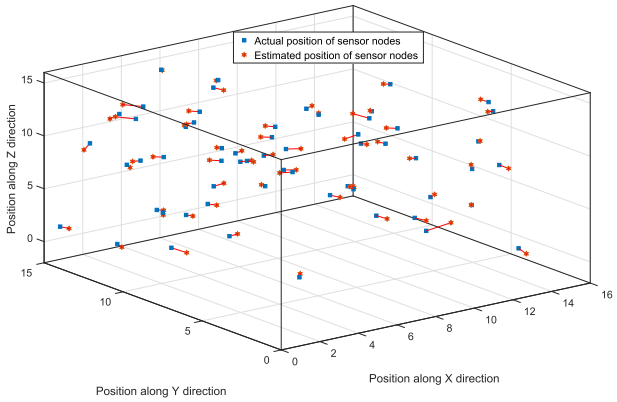

(a) Proposed technique

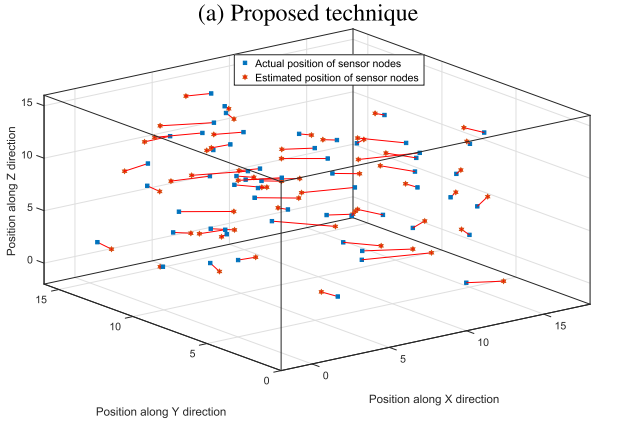

(b) LLE method [25]

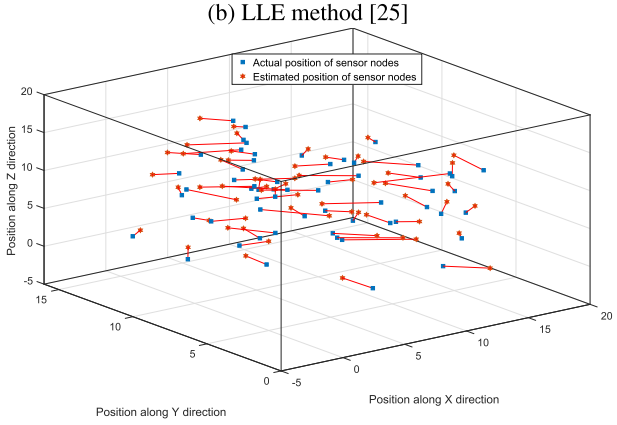

(c) WMDS method [24]

FIGURE 5. (a) Proposed technique with RMSE of 0.45 m; (b) LLE method with RMSE of 1.6 m; (c) WMDS method with RMSE of 3.21 m.

B. COMPARISON OF LOCALIZATION ACCURACY

In this subsection, we compare the localization accuracy of the proposed Isomap-based localization technique with WMDS [24] and LLE [25]. Fig. 5 shows that the localization accuracy of the proposed technique is better than WMDS and LLE in the three-dimensional space. The localization accuracy of the proposed method, LLE, and WMDS is 0.45 m, 1.6 m, and 3.21 m, respectively. LLE and WMDS fail to discover the nonlinear structure of the three-dimensional network, which results in low localization accuracy. Note that for these results we kept the ranging error variance to 0.1 m and also we did not show the results for WCL due to its significant localization error (more than 10 m) for the boundary nodes.

TABLE 1. Simulation parameters.

Parameters	Values
Operating frequency	13 MHz
Fracture size	$15 \times 15 \times 15$ m^3
Depth of the fracture	1.8 Km
Coil radius	$0.01 - 0.04$ m
Number of turns in coils	$10 - 30$
Transmit power	$100 - 200$ mW
Unit length resistance of antenna	$0.01\ \Omega/m$
Temperature	418 K
Ranging error variance	$0.1 - 0.8$ m
Number of underground things	60

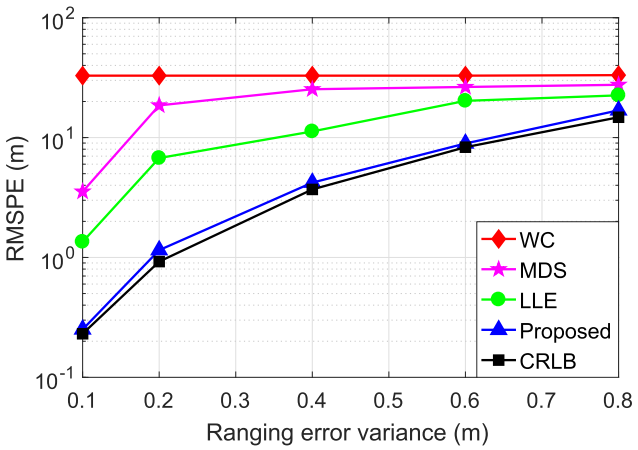

FIGURE 6. CRLB vs. Ranging error variance.

C. EFFECT OF RANGING ERROR ON LOCALIZATION ACCURACY

Fig. 6 shows the adverse effect of ranging error variance on the accuracy of the proposed localization technique for the IoUT. The ranging error and the non-availability of all pairwise distances limit the performance of every network localization scheme. Since we have assumed that the ranging error follows zero-mean Gaussian distribution with variance σ^2; therefore, we evaluate the performance of the proposed localization technique in terms of ranging error variance $\sigma^2 = 0.1 - 0.8$ m. Note that, it is common to model the ranging error as a Gaussian distribution for localization in various wireless networks. For instance, in [17] and [48], the ranging error is modeled as a Gaussian random variable with zero mean and variance σ^2 for localization in underwater optical wireless networks and underground MI-based sensor networks, respectively. Note that the results in Fig. 6 are averaged over 500 different network setups with 60 underground things randomly distributed in $15 \times 15 \times 15\ m^3$ cubic fracture. Fig. 6 shows that Isomap-based proposed technique has better localization accuracy compared to its counterparts, WC, WMDS, and LLE because the Isomap technique estimates the missing pairwise distance in three-dimensional

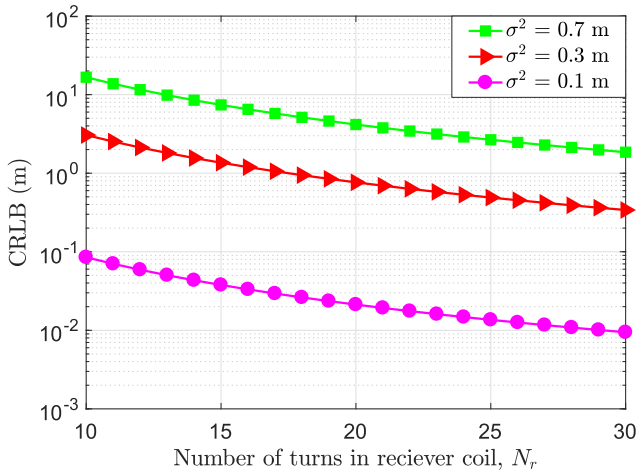

FIGURE 7. CRLB vs. Number of turns in the receiver.

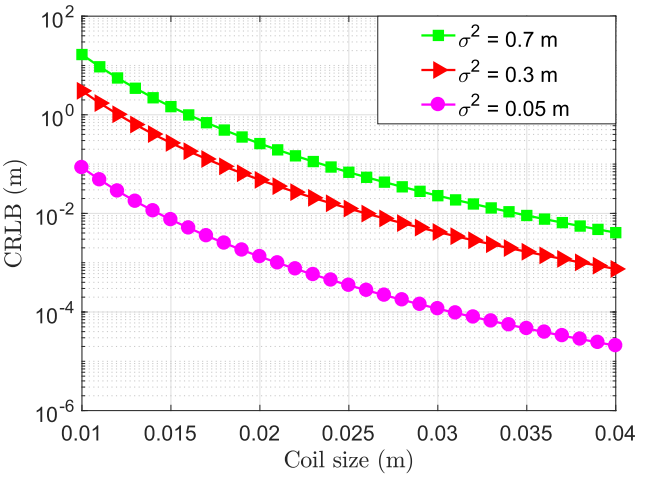

FIGURE 9. CRLB vs. Coil size.

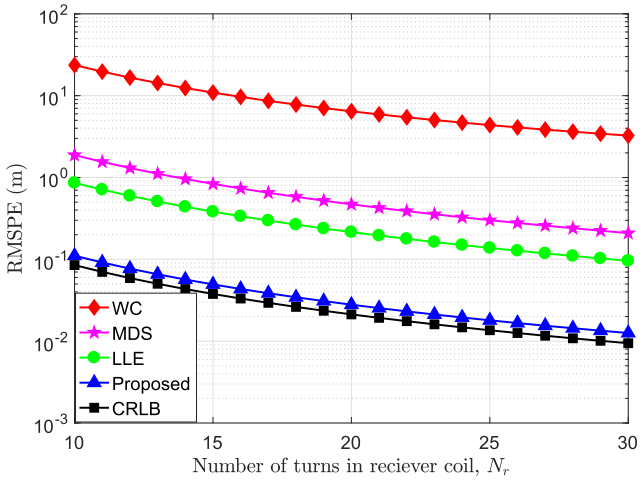

FIGURE 8. RMSPE vs. Number of turns in the receiver.

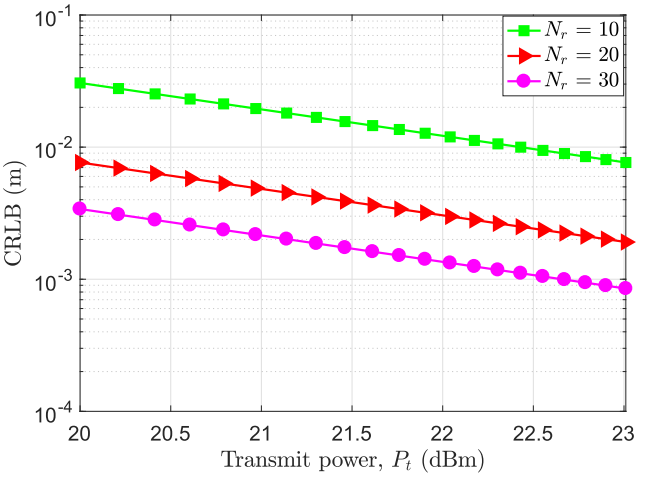

FIGURE 10. CRLB vs. Transmit power.

space more accurately by taking into account the nonlinear structure of the network.

D. EFFECT OF COIL SIZE ON LOCALIZATION ACCURACY

Fig. 7 shows CRLB as a function of the number of turns in the coil of the underground sensors. Results of CRLB in Fig. 7 are obtained at a frequency of 13 MHz with noise variances of 0.1, 0.3, and 0.7 m respectively. Fig. 7 shows that increasing the number of turns of the coils improve the localization accuracy. Moreover, to show the effect of N_r, we kept $\sigma^2 = 0.1$ m in fig. 8 and compared the results of the proposed technique with WC, WMDS, and LLE. Fig. 8 shows that increasing N_r improves the localization accuracy and due to the better estimation of missing distance, the proposed technique outperforms the traditional schemes.

Nevertheless, increasing the number of turns of the coil may increase the size of the coil where the small size of fracturing well requires small size coils. Therefore, in Fig. 9, we have investigated the impact of coil size on the performance of the achievable accuracy. It is clear from Fig. 9 that for a given ranging error variance, the achievable accuracy improves with the increase in the coil size from 0.01 m to 0.04 m. Note that the coil design parameters such as the number of turns and coil size need to be adjusted based on the results in Fig. 7 and Fig. 9 to achieve a certain localization accuracy.

E. EFFECT OF TRANSMIT POWER ON LOCALIZATION ACCURACY

Finally, we evaluate the performance of the proposed technique for MI-based IoUT regarding the transmit power. The transmit power of commercially available coils for MI communications varies from 100 mW (20 dBm) to 200 mW (23 dBm). Therefore, we kept the range of 20−23 dBm for the transmit power with the different type of coils. Fig. 10 shows that increasing the transmit power improves the achievable accuracy for a given type of coil. Moreover, we have also compared the results of the proposed technique with WC,

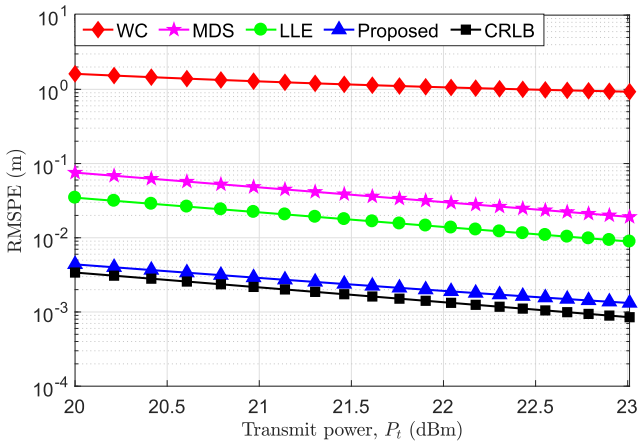

FIGURE 11. RMSPE vs. Transmit power.

WMDS, and LLE in Fig. 11 where the localization accuracy of all the techniques improves with an increase in the transmit power (for $N_r = 30$). Moreover, Fig. 11 also show that the proposed method performs better and achieves the CRLB due to better estimation of the missing distances.

According to the above results, the proposed localization technique and the CRLB is the function of MI-based channel and network parameters. Therefore, all these parameters should be taken into account to develop a robust and accurate MI-based IoUT localization system.

VII. CONCLUSION

In this paper, we propose a novel 3D localization technique based on Isometric scaling for the IoUT. Also, we derived the CRLB for the proposed MI-based localization technique. Our proposed method outperforms the traditional network localization schemes because Isometric scaling estimates the missing pairwise distances more accurately in 3D architectures. We examined the effects of numerous parameters such as the number of anchors, coil size, number of turns in the coil, ranging error, and transmit power on the performance of the proposed technique. Subsequently, we found out from our analysis that increasing the range error variance reduces the localization accuracy. Conversely, increasing the number of turns in the coil or reducing the size of the coil improves the localization accuracy. Furthermore, the effect of transmitting power is evaluated, which shows that an increase in transmit power improves the localization accuracy. The proposed 3D localization technique and the theoretical analysis and findings in this paper open the door for the development of location-aware MI-based IoUT.

APPENDIX
DERIVATION OF THE ELEMENTS FOR THE FIM

Using the PDF in (16) the partial derivatives are calculated as

$$\frac{\partial \ell_{ij}}{\partial x_i} = \frac{1}{2\sigma_{ij}^2}\left(- \frac{\partial \hat{P}_{r_j}^2}{\partial x_i} - \frac{\partial P_{r_j}^2}{\partial x_i} + \frac{\partial P_{r_j}\hat{P}_{r_j}}{\partial x_i}\right). \quad (45)$$

Putting the value of P_{r_j} in (45) yields

$$\frac{\partial \ell_{ij}}{\partial x_i} = \frac{1}{2\sigma_{ij}^2}\left(- \frac{\partial}{\partial x_i}\left(k^2 \| \mathbf{s}_i - \mathbf{s}_j \|^{-6}\right) + \hat{P}_{r_j}\frac{\partial}{\partial x_i}\left(k \| \mathbf{s}_i - \mathbf{s}_j \|^{-3}\right)\right). \quad (46)$$

Taking the partial derivative of (46) with respect to x_i yields

$$\frac{\partial \ell_{ij}}{\partial x_i} = \frac{1}{2\sigma_{ij}^2}\left(\frac{k^2 12(x_i - x_j)}{\| \mathbf{s}_i - \mathbf{s}_j \|^7} + \frac{k\hat{P}_{r_j} 6(x_i - x_j)}{\| \mathbf{s}_i - \mathbf{s}_j \|^6}\right). \quad (47)$$

Now the second-order partial derivative of (48) results in

$$\frac{\partial^2 \ell_{ij}}{\partial x_i^2} = \frac{k}{\sigma_{ij}^2}\left(\frac{6\,k}{\| \mathbf{s}_i - \mathbf{s}_j \|^7} - \frac{84\,k(x_i - x_j)^2}{\| \mathbf{s}_i - \mathbf{s}_j \|^8} + \frac{3\hat{P}_{r_j}}{\| \mathbf{s}_i - \mathbf{s}_j \|^4} - \frac{24(x_i - x_j)^2}{\| \mathbf{s}_i - \mathbf{s}_j \|^5}\right). \quad (48)$$

Now using the fact that $E(\hat{P}_{r_j}) = P_{r_j}$, (48) is simplified as

$$E\left(\frac{\partial^2 \ell_{ij}}{\partial x_i^2}\right) = \frac{3\,k}{\sigma_{ij}^2}\left(\frac{2\,k}{\| \mathbf{s}_i - \mathbf{s}_j \|^7} - \frac{28\,k(x_i - x_j)^2}{\| \mathbf{s}_i - \mathbf{s}_j \|^8} + \frac{k}{\| \mathbf{s}_i - \mathbf{s}_j \|^7} - \frac{8(x_i - x_j)^2}{\| \mathbf{s}_i - \mathbf{s}_j \|^8}\right). \quad (49)$$

Similarly, the other terms can be easily obtained as follows

$$E\left(\frac{\partial^2 \ell_{ij}}{\partial y_i^2}\right) = \frac{3k}{\sigma_{ij}^2}\left(\frac{2k}{\| \mathbf{s}_i - \mathbf{s}_j \|^7} - \frac{28k(y_i - y_j)^2}{\| \mathbf{s}_i - \mathbf{s}_j \|^8} + \frac{k}{\| \mathbf{s}_i - \mathbf{s}_j \|^7} - \frac{8(y_i - y_j)^2)}{\| \mathbf{s}_i - \mathbf{s}_j \|^5}\right), \quad (50)$$

$$E\left(\frac{\partial^2 \ell_{ij}}{\partial z_i^2}\right) = \frac{3k}{\sigma_{ij}^2}\left(\frac{2k}{\| \mathbf{s}_i - \mathbf{s}_j \|^7} - \frac{28k(z_i - z_j)^2}{\| \mathbf{s}_i - \mathbf{s}_j \|^8} + \frac{k}{\| \mathbf{s}_i - \mathbf{s}_j \|^7} - \frac{8(z_i - z_j)^2)}{\| \mathbf{s}_i - \mathbf{s}_j \|^5}\right) \quad (51)$$

$$E\left(\frac{\partial^2 \ell_{ij}}{\partial x_i y_i}\right) = \frac{60\,k^2(x_i - x_j)(y_i - y_j)}{\sigma_{ij}^2 \| \mathbf{s}_i - \mathbf{s}_j \|^8}, \quad (52)$$

$$E\left(\frac{\partial^2 \ell_{ij}}{\partial x_i z_i}\right) = \frac{60\,k^2(x_i - x_j)(z_i - z_j)}{\sigma_{ij}^2 \| \mathbf{s}_i - \mathbf{s}_j \|^8}, \quad (53)$$

$$E\left(\frac{\partial^2 \ell_{ij}}{\partial y_i z_i}\right) = \frac{60\,k^2(y_i - y_j)(z_i - z_j)}{\sigma_{ij}^2 \| \mathbf{s}_i - \mathbf{s}_j \|^8}. \quad (54)$$

The non-diagonal terms can also be obtained in the similar fashion. Finally all these derived elements complete the FIM for the CLRB.

ACKNOWLEDGMENT

The authors would like to thank the anonymous reviewers for their fruitful comments.

REFERENCES

[1] *Dynamic Communications for Oil & Gas*, Alcatel-Lucent, Helsinki, Finland, 2013.

[2] W. C. Lyons and G. J. Plisga, *Standard Handbook of Petroleum and Natural Gas Engineering*, 3rd ed. Houstan, TX, USA: Gulf Professional, 2016.

[3] S. Kisseleff, I. F. Akyildiz, and W. H. Gerstacker, "Survey on advances in magnetic induction-based wireless underground sensor networks," *IEEE Internet Things J.*, vol. 5, no. 6, pp. 4843–4856, Sep. 2018.

[4] S. Chen, H. Xu, D. Liu, B. Hu, and H. Wang, "A vision of IoT: Applications, challenges, and opportunities with china perspective," *IEEE Internet Things J.*, vol. 1, no. 4, pp. 349–359, Aug. 2014.

[5] J. J. Sojdehei, P. N. Wrathall, and D. F. Dinn, "Magneto-inductive (MI) communications," in *Proc. MTS/IEEE Conf. Exhibit.*, vol. 1, Nov. 2001, pp. 513–519.

[6] R. Bansal, "Near-field magnetic communication," *IEEE Antennas Propag. Mag.*, vol. 46, no. 2, pp. 114–115, Apr. 2004.

[7] I. F. Akyildiz and E. P. Stuntebeck, "Wireless underground sensor networks: Research challenges," *Ad Hoc Netw.*, vol. 4, no. 6, pp. 669–686, Nov. 2006.

[8] Z. Sun and I. F. Akyildiz, "Optimal deployment for magnetic induction-based wireless networks in challenged environments," *IEEE Trans. Wireless Commun.*, vol. 12, no. 3, pp. 996–1005, Mar. 2013.

[9] X. Tan, Z. Sun, and I. F. Akyldiz, "Wireless underground sensor networks: MI-based communication systems for underground applications," *IEEE Antennas Propag. Mag.*, vol. 57, no. 4, pp. 74–87, Aug. 2015.

[10] A. Charaf and G. Rodriguez-Guisantes, "Channel models in the near field," in *Proc. 11th Eur. Conf. Antennas Propag. (EUCAP)*, Mar. 2017, pp. 2861–2865.

[11] V. Pathak, V. Kumar, and R. K. Barik, "Magnetic induction communication based transceiver coil and waveguide structure modeling for non-conventional WSNs," in *Proc. Int. Conf. Comput., Commun. Netw. Technol. (ICCCNT)*, Jul. 2018, pp. 1–7.

[12] L. Yan, D. Wei, M. Pan, and J. Chen, "Downhole wireless communication using magnetic induction technique," in *Proc. United States Nat. Committee URSI Nat. Radio Sci. Meeting (USNC-URSI NRSM)*, Jan. 2018, pp. 1–2.

[13] A. Salam, M. C. Vuran, X. Dong, C. Argyropoulos, and S. Irmak, "A theoretical model of underground dipole antennas for communications in Internet of underground things," *IEEE Trans. Antennas Propag.*, vol. 67, no. 6, pp. 3996–4009, Jun. 2019.

[14] N. Saeed, T. Y. Al-Naffouri, and M.-S. Alouini, "Towards the Internet of underground things: A systematic survey," *IEEE Commun. Surveys Tuts.*, to be published.

[15] T. E. Abrudan, O. Kypris, N. Trigoni, and A. Markham, "Impact of rocks and minerals on underground magneto-inductive communication and localization," *IEEE Access*, vol. 4, pp. 3999–4010, 2016.

[16] N. G. Franconi, A. P. Bunger, E. Sejdić, and M. H. Mickle, "Wireless communication in oil and gas wells," *Energy Technol.*, vol. 2, no. 12, pp. 996–1005, Dec. 2014.

[17] S.-C. Lin, A. A. Alshehri, P. Wang, and I. F. Akyildiz, "Magnetic induction-based localization in randomly deployed wireless underground sensor networks," *IEEE Internet Things J.*, vol. 4, no. 5, pp. 1454–1465, Oct. 2017.

[18] A. K. Paul and T. Sato, "Localization in wireless sensor networks: A survey on algorithms, measurement techniques, applications and challenges," *J. Sensor Actuator Netw.*, vol. 6, no. 4, pp. 1–24, 2017.

[19] N. Saeed, A. Celik, T. Y. Al-Naffouri, and M.-S. Alouini, "Underwater optical wireless communications, networking, and localization: A survey," *Ad Hoc Netw.*, vol. 94, pp. 1–35, Jun. 2019.

[20] N. Saeed, H. Nam, T. Y. Al-Naffouri, and M. Alouini, "A state-of-the-art survey on multidimensional scaling based localization techniques," *IEEE Commun. Survey Tuts.*, to be published.

[21] A. Markham, N. Trigoni, D. W. Macdonald, and S. A. Ellwood, "Underground localization in 3-D using magneto-inductive tracking," *IEEE Sensors J.*, vol. 12, no. 6, pp. 1809–1816, Jun. 2012.

[22] H. Huang and Y. R. Zheng, "3-D localization of wireless sensor nodes using near-field magnetic-induction communications," *Phys. Commun.*, vol. 30, pp. 97–106, Oct. 2018.

[23] S. Phoemphon, C. So-In, and N. Leelathakul, "Fuzzy weighted centroid localization with virtual node approximation in wireless sensor networks," *IEEE Internet Things J.*, vol. 5, no. 6, pp. 4728–4752, Dec. 2018.

[24] Y. Ma, C. Tian, and Y. Jiang, "A multi-tag cooperative localization algorithm based on weighted multidimensional scaling for passive UHF RFID," *IEEE Internet Things J.*, to be published.

[25] N. Jain, S. Verma, and M. Kumar, "Patch-based LLE with selective neighborhood for node localization," *IEEE Sensors J.*, vol. 18, no. 9, pp. 3891–3899, May 2018.

[26] A. R. Ansari, N. Saeed, M. I. U. Haq, and S. Cho, "Accurate 3D localization method for public safety applications in vehicular ad-hoc networks," *IEEE Access*, vol. 6, pp. 20756–20763, Apr. 2018.

[27] Z. Duan and Q. Zhou, "CRLB-weighted intersection method for target localization using AOA measurements," in *Proc. IEEE Int. Conf. Comput. Intell. Virtual Environ. Meas. Syst. Appl. (CIVEMSA)*, Jun. 2015, pp. 1–6.

[28] A. Dersan and Y. Tanik, "Passive radar localization by time difference of arrival," in *Proc. MILCOM*, vol. 2, Oct. 2002, pp. 1251–1257.

[29] B. S. Çiftler, A. Kadri, and I. Güvenç, "Fundamental bounds on RSS-based wireless localization in passive UHF RFID systems," in *Proc. IEEE Wireless Commun. Netw. Conf. (WCNC)*, Mar. 2015, pp. 1356–1361.

[30] N. Patwari, A. O. Hero, M. Perkins, N. S. Correal, and R. J. O'dea, "Relative location estimation in wireless sensor networks," *IEEE Trans. Signal Process.*, vol. 51, no. 8, pp. 2137–2148, Jul. 2003.

[31] T. Jia and R. M. Buehrer, "A new Cramer-Rao lower bound for TOA-based localization," in *Proc. IEEE Military Commun. Conf.*, Nov. 2008, pp. 1–5.

[32] N. Saeed and H. Nam, "Cluster based multidimensional scaling for irregular cognitive radio networks localization," *IEEE Trans. Signal Process.*, vol. 64, no. 10, pp. 2649–2659, May 2016.

[33] H. Guo and Z. Sun, "Channel and energy modeling for self-contained wireless sensor networks in oil reservoirs," *IEEE Trans. Wireless Commun.*, vol. 13, no. 4, pp. 2258–2269, Apr. 2014.

[34] M. A. Akkaş, "Channel modeling of wireless sensor networks in oil," *Wireless Pers. Commun.*, vol. 95, no. 4, pp. 4337–4355, Aug. 2017.

[35] Z. Sun and I. F. Akyildiz, "Underground wireless communication using magnetic induction," in *Proc. IEEE Int. Conf. Commun.*, Jun. 2009, pp. 1–5.

[36] E. W. Dijkstra, "A note on two problems in connexion with graphs," *Numer. Math.*, vol. 1, no. 1, pp. 269–271, Dec. 1959.

[37] S. Li, Y. Sun, and W. Shi, "Capacity of magnetic-induction MIMO communication for wireless underground sensor networks," *Int. J. Distrib. Sensor Netw.*, vol. 11, Oct. 2015, Art. no. 426324.

[38] X.-Y. Li, W.-Z. Song, and Y. Wang, "Localized topology control for heterogeneous wireless sensor networks," *ACM Trans. Sensor Netw.*, vol. 2, no. 1, pp. 129–153, Feb. 2006.

[39] N. Saeed, H. Nam, M. I. U. Haq, and D. B. M. Saqib, "A survey on multidimensional scaling," *ACM Comput. Surv.*, vol. 51, no. 3, pp. 1–25, 2018.

[40] J. B. Tenenbaum, V. de Silva, and J. C. Langford, "A global geometric framework for nonlinear dimensionality reduction," *Science*, vol. 290, no. 5500, pp. 2319–2323, Dec. 2000.

[41] J. B. Kruskal, "Multidimensional scaling by optimizing goodness of fit to a nonmetric hypothesis," *Psychometrika*, vol. 29, no. 1, pp. 1–27, Mar. 1964.

[42] G. A. Watson, "Computing helmert transformations," *J. Comput. Appl. Math.*, vol. 197, no. 2, pp. 387–394, 2006.

[43] F. Crosilla, A. Beinat, A. Fusiello, E. Maset, and D. Visintini, *Orthogonal Procrustes Analysis*. Cham, Switzerland: Springer, 2019, pp. 7–28.

[44] H. L. Van Trees and K. L. Bell, *Bayesian Bounds for Parameter Estimation and Nonlinear Filtering/Tracking*. New York, NY, USA: Wiley, 2007.

[45] H. L. van Trees, *Detection, Estimation, and Modulation Theory, Part I: Detection, Estimation, and Linear Modulation Theory*. Hoboken, NJ, USA: Wiley, 2004.

[46] P. Pakrooh, A. Pezeshki, L. L. Scharf, D. Cochran, and S. D. Howard, "Analysis of Fisher information and the Cramér–Rao bound for nonlinear parameter estimation after random compression," *IEEE Trans. Signal Process.*, vol. 63, no. 23, pp. 6423–6428, Dec. 2015.

[47] M. A. Grant, I. G. Donaldson, and P. F. Bixley, *Geothermal Reservoir Engineering*. New York, NY, USA: Academic, 1982.

[48] N. Saeed, A. Celik, T. Y. Al-Naffouri, and M.-S. Alouini, "Localization of energy harvesting empowered underwater optical wireless sensor networks," *IEEE Trans. Wireless Commun.*, vol. 18, no. 5, pp. 2652–2663, May 2019.

NASIR SAEED (S'14–M'16–SM'19) received the bachelor's degree in telecommunication from the University of Engineering and Technology, Peshawar, Pakistan, in 2009, the master's degree in satellite navigation from Polito di Torino, Italy, in 2012, and the Ph.D. degree in electronics and communication engineering from Hanyang University, Seoul, South Korea, in 2015. He was an Assistant Professor with the Department of Electrical Engineering, Gandhara Institute of Science and IT, Peshawar, from August 2015 to September 2016. He was an Assistant Professor with IQRA National University, Peshawar, from July 2017 to October 2017. He is currently a Postdoctoral Research Fellow with the King Abdullah University of Science and Technology (KAUST). His current research interests include cognitive radio networks, underwater optical wireless communications, underground communications, dimensionality reduction, and localization.

MOHAMED-SLIM ALOUINI (S'94–M'98–SM'03–F'09) was born in Tunis, Tunisia. He received the Ph.D. degree in electrical engineering from the California Institute of Technology (Caltech), Pasadena, CA, USA, in 1998. He served as a Faculty Member with the University of Minnesota, Minneapolis, MN, USA, Texas A&M University at Qatar, Doha, Qatar. In 2009, he joined the King Abdullah University of Science and Technology (KAUST), Thuwal, Makkah, Saudi Arabia, as a Professor of electrical engineering. His current research interests include the modeling, design, and performance analysis of wireless communication systems.

TAREQ Y. AL-NAFFOURI (M'10–SM'18) received the B.S. degree (Hons.) in mathematics and electrical engineering from the King Fahd University of Petroleum and Minerals, Dhahran, Saudi Arabia, the M.S. degree in electrical engineering from the Georgia Institute of Technology, Atlanta, GA, USA, in 1998, and the Ph.D. degree in electrical engineering from Stanford University, Stanford, CA, USA, in 2004.

He has held internship positions with NEC Research Labs, Tokyo, Japan, in 1998, the Adaptive Systems Lab, University of California at Los Angeles, in 1999, National Semiconductor, Santa Clara, CA, USA, in 2001 and 2002, and Beceem Communications Santa Clara, in 2004. He was a Visiting Scholar with the California Institute of Technology, Pasadena, CA, USA, in 2005 and summer 2006. He was a Fulbright Scholar with the University of Southern California, in 2008. He is currently an Associate Professor with the Electrical Engineering Department, King Abdullah University of Science and Technology (KAUST). He has over 240 publications in journal and conference proceedings, nine standard contributions, 14 issued patents, and eight pending. His research interests include sparse, adaptive, statistical signal processing and their applications, localization, machine learning, and network information theory. He was the recipient of the IEEE Education Society Chapter Achievement Award, in 2008, and the Al-Marai Award for Innovative Research in Communication, in 2009. He has also been serving as an Associate Editor for the TRANSACTIONS ON SIGNAL PROCESSING, since August 2013.